Rapid Communications

Honeycomb lattice type charge density wave associated with interlayer Cu ions ordering in $1T$-Cu_xTiSe_2

Shunsuke Kitou,[1,2] Shintaro Kobayashi,[1] Tatsuya Kaneko,[3] Naoyuki Katayama,[1]
Seiji Yunoki,[3,4,5] Toshikazu Nakamura,[2] and Hiroshi Sawa[1,*]

[1]*Department of Applied Physics, Nagoya University, Nagoya 464-8603, Japan*
[2]*Institute for Molecular Science, Myodaiji, Okazaki 444-8585, Japan*
[3]*Computational Condensed Matter Physics Laboratory, RIKEN Cluster for Pioneering Research (CPR), Wako, Saitama 351-0198, Japan*
[4]*Computational Quantum Matter Research Team, RIKEN Center for Emergent Matter Science (CEMS), Wako, Saitama 351-0198, Japan*
[5]*Computational Materials Science Research Team, RIKEN Center for Computational Science (R-CCS), Kobe, Hyogo 650-0047, Japan*

(Received 9 October 2018; revised manuscript received 29 January 2019; published 11 February 2019)

The phase transition phenomenon in a semimetallic $1T$-$TiSe_2$ has attracted attention as an excitonic insulator. However, as the phase transition accompanying superlattice peaks has the q vector connecting the Fermi surfaces of the three-dimensional shape of hole and electron pockets, it also assumes the charge density wave (CDW) state owing to the electron–phonon interaction. To understand the electronic state at the low temperature, control of the chemical potential was attempted by electronic doping through Cu^+ intercalation. Physical properties measurements and synchrotron x-ray diffraction experiments in Cu_xTiSe_2 ($x = 0$–0.35) were performed. The phase transition was determined to occur as a cooperative phenomenon between the honeycomb lattice type CDW corresponding to the nesting vector and the ordered state of the Cu^+ ions between $TiSe_2$ layers at a specific doping amount ($x = 1/3$). The behavior of Cu^+ ions in highly doped regions suggests the occurrence of a two-dimensional liquid-solid state transition based on the temperature dependence of the x-ray diffuse scattering.

DOI: 10.1103/PhysRevB.99.081111

Introduction. The study of charge density waves (CDWs) is a longstanding but still attractive research topic in condensed matter physics [1]. Transition-metal dichalcogenide (TMD) series show various CDW states, such as the incommensurate-CDW state in $2H$-$NbSe_2$ [2] and Star-of-David clusters in $1T$-TaS_2 [3]. Moreover, as TMDs have two-dimensional (2D) layered structures, their electronic states can be controlled by intercalation or pressure, and superconductivity (SC) frequently appears around the CDW state [4].

From this viewpoint, $1T$-$TiSe_2$, which shows a characteristic triple-q CDW state [5–7], is an interesting stage, in which a second-order phase transition with a superlattice structure of $2\boldsymbol{a}_\alpha \times 2\boldsymbol{b}_\alpha \times 2\boldsymbol{c}_\alpha$ is known to occur from the semimetal state (α phase) to the triple-q CDW state (β phase) at the β phase transition temperature $T_\beta \approx 200$ K [8]. This is because of the ordering of vectors between hole pockets of the Se-4p band at the Γ point and electron pockets of the Ti-3d band at the L points [9]. However, as the Fermi surface (FS) in $1T$-$TiSe_2$ has 3D shapes and the size of two Fermi surfaces contributing to the nesting between electron and hole is different, the triple-q nesting condition is not satisfactory and the CDW is not simple. In this CDW phase transition, the softening of the transverse optical phonon mode is observed by the inelastic x-ray scattering measurement [10]. This is a mode in which Ti and Se vibrate in the opposite direction in the plane and this structure is not accounted for by the charge disproportionation in the unit cell. Thus, the electron-hole (excitonic) interaction [11–15] and/or the electron-phonon coupling (EPC) [5–7,10,16,17] are considered important in this phase transition; however, this mechanism is still controversial.

This characteristic electronic state in $1T$-$TiSe_2$ can be changed through Cu intercalation corresponding to electron doping from Cu atoms to $1T$-$TiSe_2$. Indeed, the SC in Cu_xTiSe_2 was reported at $0.04 \leqslant x \leqslant 0.10$ ($T_{SC}^{max} = 4.15$ K in $x = 0.08$) [18]. Many experiments and theoretical calculations about this electronic state have been actively performed [19–28] and are actively being conducted. In addition, the SC was also reported in this system by pressure [29] and electric field effect [30].

In contrast to well-studied Cu_xTiSe_2 on the low-doped region, only a few studies have reported on the Cu_xTiSe_2 in high-doped regions ($x > 0.10$) [31–33]. It is interesting how the electronic state of $1T$-$TiSe_2$, comprising two carriers of electrons and holes, would change if the chemical potential was greatly moved by electron high doping from Cu atoms.

In this work, we succeeded in synthesizing single-crystal samples of Cu_xTiSe_2 ($x = 0$–0.35) and measured physical properties and analyzed the crystal structure through synchrotron x-ray diffraction (XRD). We found that $x = 1/4$ and $1/3$ were magic numbers in this system and phase transitions were caused by the interaction among Cu atoms.

Experiment. Eleven kinds of Cu_xTiSe_2 samples were synthesized with reference to a previous study [31]. The amount of Cu in Cu_xTiSe_2 was determined through the crystal structural analysis by using synchrotron XRD. DC magnetization measurements were conducted using a superconducting

*Corresponding author: z47827a@cc.nagoya-u.ac.jp

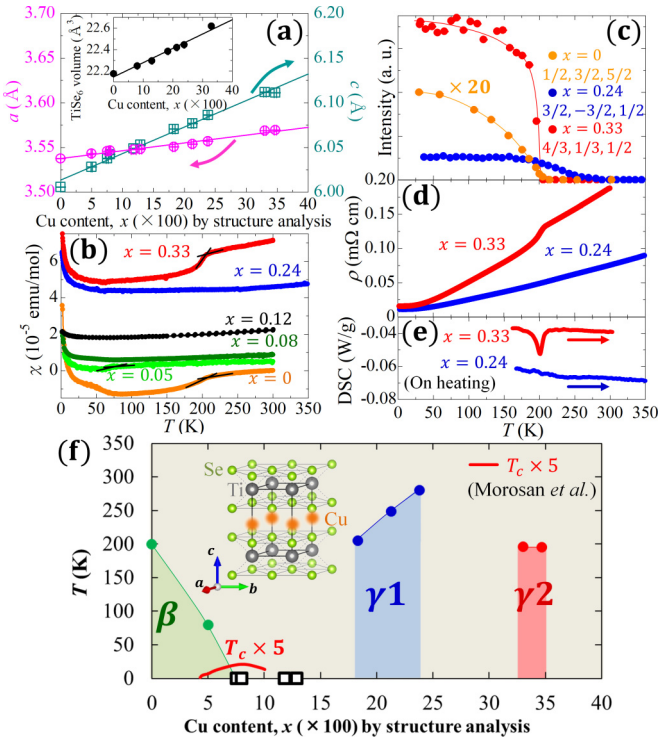

FIG. 1. (a) Lattice parameters of Cu_xTiSe_2 in $0 \leqslant x \leqslant 0.35$ at room temperature. Inset: The volume of $TiSe_6$ octahedrons. (b) Temperature dependence of the magnetic susceptibility under 1 or 5 T. (c) Temperature dependence of the intensity of the superlattice reflections for $x = 0$, 0.24, and 0.33. The intensity in $x = 0$ is shown as 20 times larger. The intensity of superlattice reflections is scaled with the intensity of each main reflection (0, 0, 2) at 30 K. (d),(e) Temperature dependence of the electric resistivity, and the DSC signals. (f) The x–T phase diagram of Cu_xTiSe_2. The superconductivity dome represented by the red line is taken from Ref. [18]. White squares indicate that there are no superlattice reflections and no diffuse scattering above 25 K from our XRD experiments. The crystal structure of Cu_xTiSe_2 in the high-temperature phase is also shown in the figure.

quantum interference device magnetometer in a Quantum Design MPMS instrument. Electric resistivity measurements were performed in a Quantum Design PPMS instrument by using the standard four-probe technique. Differential scanning calorimetry (DSC) was performed using DSC 204F1 Phoenix (Netzsch). The XRD experiments were conducted using a BL02B1 beam line equipped at the synchrotron facility SPring-8 in Japan [34]. A helium-gas-blowing device was employed to decrease the temperature to 25 K. A CCD camera, PILATUS, or 2D imaging plate was used as the diffractometer's detector. A density-functional-theory (DFT) calculation was performed using the full-potential linearized augmented-plane-wave method with the generalized gradient approximation [35] in the WIEN2K code [36].

Result and discussion. Figure 1(a) shows lattice parameters of Cu_xTiSe_2 in $0 \leqslant x \leqslant 0.35$ at room temperature (RT). By increasing x, the c-axis parameter remarkably increases, while the a-axis parameter also monotonically increases. These results are consistent with the reported data [18,31]. Diffuse streaks with a very weak intensity appeared in $\boldsymbol{a}^*\boldsymbol{b}^*$ planes in $Cu_{0.33}TiSe_2$, and $Cu_{0.35}TiSe_2$ at RT in the XRD data (see Supplemental Material [37]); however, the crystal structural analysis was performed by ignoring this intensity. A crystal structure, which was almost the same as that of $1T$-$TiSe_2$ at the high-temperature phase ($P\bar{3}m1$), was confirmed for each Cu_xTiSe_2 in $0 \leqslant x \leqslant 0.35$ [inset of Fig. 1(f)]. Cu exists at the $1b$ site (Wyckoff letter), which is the site between $TiSe_2$ layers. The inset of Fig. 1(a) shows the volume of $TiSe_6$ octahedrons at RT. The $TiSe_6$ volume corresponding to the ionic radius of Ti increases with the increase in x, indicating the decrease of the valence of Ti. This corresponds to the electron doping from Cu atoms to $TiSe_2$ layers. This electron doping has also been verified through the DFT calculation [38] (see Supplemental Material [37]).

Figure 1(b) shows the magnetic susceptibility of Cu_xTiSe_2. The magnetic susceptibility increases with increasing x at RT, which suggests the enhanced Pauli paramagnetic contribution from the itinerant electrons. The density of state (DOS) in the $TiSe_2$ layers is assumed to increase because of electron doping. The magnetic susceptibility for $x \leqslant 0.08$ is in good agreement with the reported data [18] and the SC was also confirmed from our measurements in $x = 0.05$ and 0.08. Decreases in the magnetic susceptibility corresponding to the β phase transition were confirmed at 200 and 80 K in $x = 0$ and 0.05, respectively, but not in $0.08 \leqslant x \leqslant 0.24$. In addition, a clear decrease in magnetic susceptibility was confirmed at approximately 200 K in $x = 0.33$.

The temperature dependence of the XRD data was investigated for each x content in Cu_xTiSe_2. The superlattice reflections corresponding to the β phase ($2\boldsymbol{a}_\alpha \times 2\boldsymbol{b}_\alpha \times 2\boldsymbol{c}_\alpha$: $P\bar{3}c1$) were observed at $T_\beta \approx 200$ and 80 K for $x = 0$ [Fig. 1(c)] and 0.05, respectively. This result is consistent with the previous XRD data [27]. The β phase transition was suppressed with increasing x and was not observed in $0.08 \leqslant x \leqslant 0.13$ above 25 K. Although this is not consistent with the previous XRD data [27], the present data shows good agreement with the previous result of Raman scattering [23] and inelastic x-ray scattering [25]. One possible scenario is that as the hole carrier at the Γ point is reduced because of electron doping from Cu atoms, the energy gain due to the excitonic interaction decreases and the β phase transition is suppressed [19,20].

In $x = 0.18$, 0.21, and 0.24, superlattice reflections corresponding to $2\boldsymbol{a}_\alpha \times 2\boldsymbol{b}_\alpha \times 2\boldsymbol{c}_\alpha$, the unit cell size of which is the same as that of the β phase, were observed at $T_{\gamma 1} \approx 205$, 250, and 280 K, respectively. The blue dots in Fig. 1(c) show the temperature dependence of the intensity of a superlattice reflection (3/2, −3/2, 1/2) of $Cu_{0.24}TiSe_2$. This intensity (3/2, −3/2, 1/2) is approximately four times that of the intensity (1/2, 3/2, 5/2) of $1T$-$TiSe_2$. Furthermore, their temperature dependences differ. Later in the text, we show that the origin of the new $\gamma 1$ phase transition is different from the β phase transition.

Moreover, another phase was confirmed in higher-doped regions of Cu. In $x = 0.33$ and 0.35, superlattice reflections corresponding to the $\sqrt{3}\boldsymbol{a}_\alpha \times \sqrt{3}\boldsymbol{b}_\alpha \times 2\boldsymbol{c}_\alpha$ structure were observed at $T_{\gamma 2} \approx 200$ K. This new $\gamma 2$ phase has a different superlattice structure from the β and $\gamma 1$ phases. Intensity (4/3, 1/3, 1/2) of $Cu_{0.33}TiSe_2$ [red dots in Fig. 1(c)] sharply increased from approximately 200 K and is approximately seven times stronger than that of $Cu_{0.24}TiSe_2$.

The results so far are summarized as the x–T phase diagram in Fig. 1(f). In the present study, we could not prepare Cu_xTiSe_2 samples with $0.24 < x < 0.33$ and $x > 0.35$. Even if we tried to synthesize single crystals with $0.24 < x < 0.33$, the synthesized sample was always $x < 0.24$ or $x > 0.33$. In our synthesis method, it is considered that phase separation occurs in the region of $0.24 < x < 0.33$. To investigate the difference between the physical properties for $Cu_{0.24}TiSe_2$ and $Cu_{0.33}TiSe_2$, the temperature dependence of the electric resistivity and the DSC signals was measured [Figs. 1(d) and 1(e)]. The behavior of the phase transitions greatly differs between $Cu_{0.24}TiSe_2$ and $Cu_{0.33}TiSe_2$. The change corresponding to the $\gamma 1$ phase transition could not be confirmed from the magnetic susceptibility, the electric resistivity, and the DSC signals in $Cu_{0.24}TiSe_2$, whereas clear signals were obtained at $T_{\gamma 2} \approx 200$ K for $Cu_{0.33}TiSe_2$. The electric resistivity shows a discontinuous decrease at $T_{\gamma 2}$ in $Cu_{0.33}TiSe_2$. A sharp peak was observed from DSC signals and the increase of entropy was $\Delta S = 0.96\,\mathrm{J\,mol^{-1}\,K^{-1}}$ in $Cu_{0.33}TiSe_2$. Although this behavior appeared as a first-order transition, the hysteresis loop was not observed to occur around $T_{\gamma 2}$ in $Cu_{0.33}TiSe_2$ from the magnetic susceptibility and the electric resistivity. In addition, the SC was absent down to 120 mK for all samples with $x \geqslant 0.13$ in the electric resistivity measurement.

To understand the difference in the electrical states for the $\gamma 1$ and $\gamma 2$ phases, we performed synchrotron XRD experiments. First, we show the XRD pattern and the results of the structural analysis for $Cu_{0.33}TiSe_2$ with stronger intensity of superlattice reflections. Figures 2(a)–2(c) show the XRD data in-plane of $Cu_{0.33}TiSe_2$. The insets of Figs. 2(a) and 2(c) show the data in the $\boldsymbol{c}^*$ direction. At 205 K, the diffuse streaks appear in the in-plane directions; this does not spread along the $\boldsymbol{c}^*$ direction. The intensity of the diffuse scattering develops toward the $\gamma 2$ phase transition. The XRD data of Fig. 2(b) will be mentioned later. Below $T_{\gamma 2}$, the diffuse streaks condense to form superlattice reflections [Fig. 2(c)], resulting in a unit cell of $\sqrt{3}\boldsymbol{a}_{\boldsymbol{\alpha}} \times \sqrt{3}\boldsymbol{b}_{\boldsymbol{\alpha}} \times 2\boldsymbol{c}_{\boldsymbol{\alpha}}$. In contrast, the very weak diffuse streaks appear in the $\boldsymbol{c}^*$ direction. This implies that the complete order state is realized in-plane, whereas the disorder remains in the stacking direction in the $\gamma 2$ phase. In this case, as the extinction rule of c-glide ($hh\bar{2}hl$: $l = 2n + 1$) exists in the pattern of superlattice reflections and the disappearance of the inversion center is not confirmed, we conclude that the space group is $P\bar{3}1c$.

As the full width at half maximum of the superlattice reflections in the $\boldsymbol{c}^*$ direction was almost the same as that of the main reflections at 30 K (see Supplemental Material [37]), the intensity of these peaks could be correctly extracted. As a result of the structural analysis including the intensity of superlattice reflections, the structure of $TiSe_2$ layers hardly changed and Cu atoms were ordered with a pattern of $\sqrt{3}\boldsymbol{a}_{\boldsymbol{\alpha}} \times \sqrt{3}\boldsymbol{b}_{\boldsymbol{\alpha}}$ in the layer [Fig. 2(d)]. In the $\gamma 2$ phase, two kinds of $TiSe_6$ octahedrons exist with volumes of 22.318 and 22.572 $\mathrm{Å}^3$, and composition ratio of 1:2. Furthermore, as Cu atoms do not exist continuously at the same (x, y) coordinates in the next layer reflecting the symmetrical operation of the c-glide, a double period is formed in the stacking direction ($2\boldsymbol{c}_{\boldsymbol{\alpha}}$).

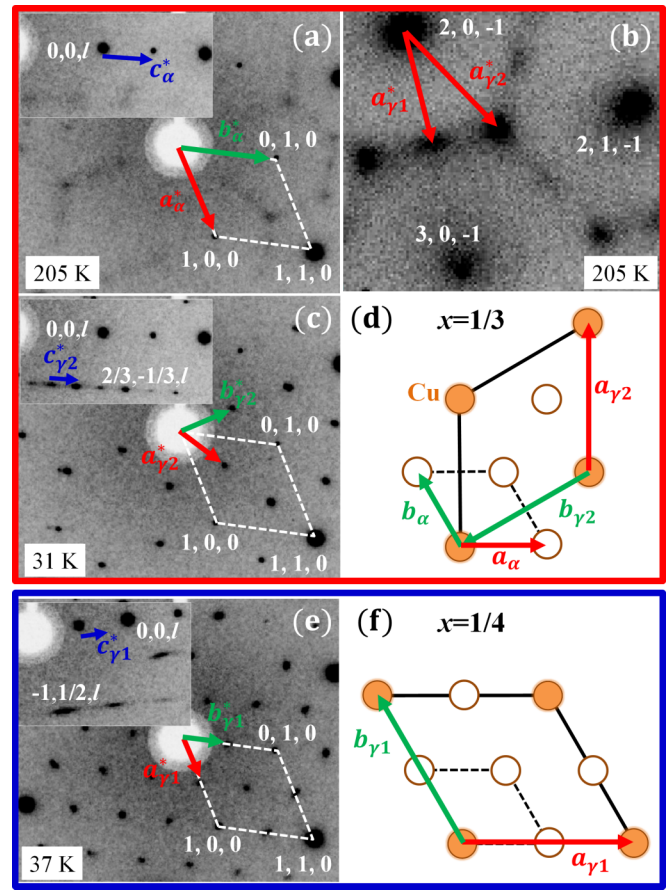

FIG. 2. (a)–(c) XRD data in-plane of $Cu_{0.33}TiSe_2$ at 205, 205 (enlarged), and 31 K, respectively. (e) XRD data in-plane of $Cu_{0.24}TiSe_2$ at 37 K. The insets of (a), (c), and (e) show the c^* direction. (d),(f) Cu-ordering patterns in $x = 1/3$ and $1/4$, respectively.

Next, we show the XRD pattern for $Cu_{0.24}TiSe_2$. Figure 2(e) shows the XRD data in-plane of $Cu_{0.24}TiSe_2$ at 37 K. The diffuse scattering was hardly observed in-plane above $T_{\gamma 1}$. Below $T_{\gamma 1}$, a superlattice structure of $2\boldsymbol{a}_{\boldsymbol{\alpha}} \times 2\boldsymbol{b}_{\boldsymbol{\alpha}} \times 2\boldsymbol{c}_{\boldsymbol{\alpha}}$ is realized in $Cu_{0.24}TiSe_2$. As these reflections break the extinction rule of c-glide ($hh\bar{0}l : l = 2n + 1$), the space group is not $P\bar{3}c1$. Thus, the $\gamma 1$ phase differs from the β phase. In this case, there was a characteristic extinction pattern (h, $k = 2n$ and $l = 2n + 1$) in the superlattice reflections. The calculated crystal structure factor [37] is consistent with the condition that Cu atoms order at an interval of $2\boldsymbol{a}_{\boldsymbol{\alpha}} \times 2\boldsymbol{b}_{\boldsymbol{\alpha}}$ in layer [Fig. 2(f)], and Cu atoms do not exist continuously at the same (x, y) coordinates in the next layer. The Cu-ordering state, which is different from the $\gamma 2$ phase, is also realized in the $\gamma 1$ phase. In the $\gamma 1$ phase, as the shape of the superlattice peaks was very broad in the $\boldsymbol{c}^*$ direction [inset of Fig. 2(e)] and their intensity was weak, the atomic positions could not be obtained even through synchrotron XRD.

Cu atoms regularly align in both the $\gamma 1$ and $\gamma 2$ phases, whereas Cu atoms exist randomly in the high-temperature phase. In other words, these transitions in $Cu_{0.24}TiSe_2$ and $Cu_{0.33}TiSe_2$ are the disorder–order transitions of Cu atoms. The decrease in the electric resistivity at $T_{\gamma 2}$ for $Cu_{0.33}TiSe_2$

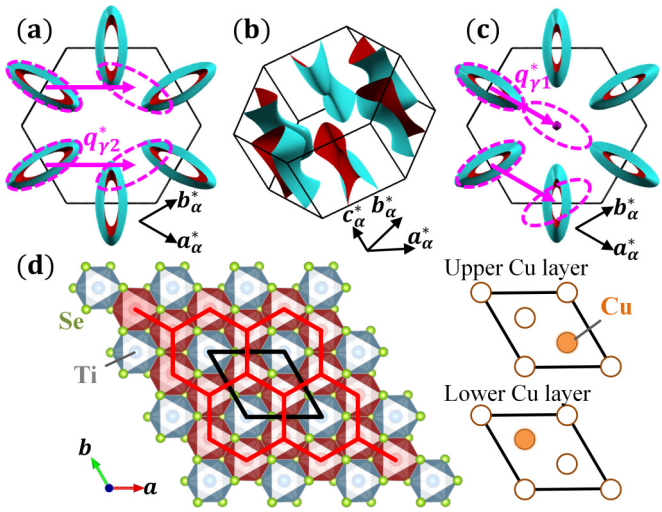

FIG. 3. Fermi surfaces of (a),(b) $Li_{0.33}TiSe_2$ and (c) $Li_{0.24}TiSe_2$ [43]. (d) The black lines show the size of the unit cell in the $\gamma 2$ phase. Left: The honeycomb lattice type CDW formation in the $\gamma 2$ phase of $Cu_{0.33}TiSe_2$ [44]. The red and blue colors indicate the electron-rich and electron-poor $TiSe_6$ octahedrons, respectively. Right: Cu-ordering pattern in upper and lower layers of the $TiSe_2$ layer.

[Fig. 1(d)] is due to the suppression of impurity scattering of Cu atoms caused by Cu ordering. However, the decrease in magnetic susceptibility at $T_{\gamma 2}$ [Fig. 1(b)] cannot be explained only by Cu ordering. The key to answer this question is the relationship between the Cu-ordering pattern in a real space and the FS in an inverse space. Thus, we estimated the FS based on the DFT calculation. Here, we employed the virtual crystal approximation (VCA) [39–41] to estimate the FS in the original Brillouin zone at the high-temperature phase. As the electron configuration of Cu atoms is unsuitable in the VCA to realize electron doping from intercalated atoms to $TiSe_2$ layers corresponding to the supercell calculations, we substituted Cu ($3d^{10}$, $4s^1$) with Li ($2s^1$) having the same number of electrons in the s orbitals and almost the same ion radius [42]. Details and validity of the calculations are noted in the Supplemental Material [37].

Figures 3(a) and 3(b) show the FS (mainly Ti-3d) of electrons in $Li_{0.33}TiSe_2$ at RT. In $Li_{0.33}TiSe_2$, there are no hole pockets [37], which means no excitonic interaction. Nesting vectors $\boldsymbol{q}^*_{\gamma 2} = \boldsymbol{a}^*_{\gamma 2} + \boldsymbol{c}^*_{\gamma 2}$ corresponding to the superlattice structures of the $\gamma 2$ phase are shown on the FS of $Li_{0.33}TiSe_2$. In this case, three kinds of $\boldsymbol{q}^*_{\gamma 2}$ vectors exist at every 120°. A partial overlap of the FS was observed due to nesting. The ratio of the FS overlap due to the $\gamma 2$ phase transition is approximately 1/6, which is about the same as the decreasing value of the magnetic susceptibility [Fig. 1(b)].

As an energy gain is observed due to nesting (imperfect nesting) in $Cu_{0.33}TiSe_2$, the CDW state in the $TiSe_2$ layers is realized. Indeed, two kinds of $TiSe_6$ octahedrons with different volumes, that is, electron rich (large $TiSe_6$) and electron poor (small $TiSe_6$) described by red and blue in Fig. 3(d), are confirmed from our results of the structural analysis. This atomic displacement in $Cu_{0.33}TiSe_2$ is different from the triple-q CDW mode in pristine 1T-$TiSe_2$ [5–7]. Focusing on a $TiSe_2$ layer, this is a honeycomb lattice type CDW formation. In $Cu_{0.33}TiSe_2$, a hybrid type CDW phase transition is realized through this commensurate connection between the Cu ordering in real space and the nesting of the FS in inverse space. Thus, $x = 1/3$ is a magic number in this system. This honeycomb lattice type CDW in $TiSe_2$ layers for $Cu_{0.33}TiSe_2$, in which there is no excitonic interaction, is completely different from the triple-q CDW caused by the excitonic interaction and/or the EPC in nondoped 1T-$TiSe_2$.

Considering the nesting condition in $Cu_{0.24}TiSe_2$, only point or line contacts of FS could be observed [Fig. 3(c)] and there is little energy gain due to nesting. This is why the change of the magnetic susceptibility was hardly observed at $T_{\gamma 1}$ [Fig. 1(b)]. Thus, pure Cu ordering is thought to be realized in the $\gamma 1$ phase, in which there seems to be no CDW. The ordering of Cu atoms is the driving force for both the $\gamma 1$ and $\gamma 2$ phase transitions. In the $\gamma 1$ phase, the amount of Cu is smaller and the distance among Cu atoms in the ordered state is longer than in the $\gamma 2$ phase. Since the interaction among Cu atoms is weaker and the phase transition is broader [Fig. 1(c)], the change in the electric resistivity and entropy is not observed in the $\gamma 1$ phase [Figs. 1(d) and 1(e)].

Moreover, the XRD data of $Cu_{0.33}TiSe_2$ at 205 K in Fig. 2(b) shows that the diffuse scattering corresponding to both $2\boldsymbol{a}_\alpha \times 2\boldsymbol{b}_\alpha$ and $\sqrt{3}\boldsymbol{a}_\alpha \times \sqrt{3}\boldsymbol{b}_\alpha$ coexists in-plane. This implies that two potential minimums of Cu sites exist just above $T_{\gamma 2}$. In contrast, below $T_{\gamma 2}$, the diffuse scattering corresponding to $\sqrt{3}\boldsymbol{a}_\alpha \times \sqrt{3}\boldsymbol{b}_\alpha$ condenses to form superlattice reflections, while the diffuse scattering corresponding to $2\boldsymbol{a}_\alpha \times 2\boldsymbol{b}_\alpha$ disappears. This result indicates that Cu atoms have a degree of freedom to move between sites in the high-temperature phase. This may imply a liquidlike behavior of Cu atoms in Cu_xTiSe_2 with a 2D-layered structure. Actually, the Cu^+ ion conductivity and the ion liquidlike thermal conductivity were reported in Cu_2Se with a cubic structure [45,46], and, very recently, the superionic conduction state was reported in $CuCrSe_2$ [47]. In addition, from the viewpoint that the interlayer ions behave like a liquid and the electronic state of the host structure can be controlled by the amount of x, Cu_xTiSe_2 is similar to Na_xCoO_2, which not only has various electronic properties [48,49] but also attracts attention as battery [50] and thermoelectric [51] materials. The liquid state of Cu_xTiSe_2 may be the hopping model like Na_xCoO_2. To obtain knowledge about this liquid state of Cu atoms in this system, we are planning synchrotron inelastic x-ray scattering measurements.

In summary, we demonstrated the two types of disorder-order transitions in Cu_xTiSe_2 ($x \approx 1/4$ and 1/3) by using synchrotron XRD. The ordering of Cu atoms is the driving force for these phase transitions in both the cases of the $\gamma 1$ and $\gamma 2$ phases. The difference is the absence or presence of the commensurate connection between the real and inverse spaces. In $Cu_{0.33}TiSe_2$, the honeycomb lattice type CDW formation was observed to cooperatively occur. The electronic state of 1T-$TiSe_2$ changes not only through electron doping with Cu intercalation but also through the ordering of Cu atoms. We believe that our results contribute significantly in the study of 1T-$TiSe_2$ and could open a door to the study of liquidlike behavior of Cu atoms.

Acknowledgments. We thank Y. Masubuchi, S. Tsutsui, T. Yamaguchi, and A. Nakano for fruitful discussions. This

work was supported by a Grant-in-Aid for Scientific Research (Grants No. JP17K17793, No. JP18K13509, and No. JP18H01183) from JSPS, Kato Foundation for Promotion of Science, and the Daiko Foundation. This work was carried out under the Visiting Researcher's Program of the Institute for Solid State Physics, the University of Tokyo, and the Institute for Molecular Science (IMS), supported by the Nanotechnology Platform Program (Molecule and Material Synthesis) of the Ministry of Education, Culture, Sports, Science and Technology (MEXT), Japan. The synchrotron radiation experiments were performed at SPring-8 with the approval of the Japan Synchrotron Radiation Research Institute (JASRI) (Proposals No. 2016B1270, No. 2017A1081, and No. 2017B1733).

[1] K. Rossnagel, J. Phys.: Condens. Matter **23**, 213001 (2011).
[2] D. E. Moncton, J. D. Axe, and F. J. DiSalvo, Phys. Rev. Lett. **34**, 734 (1975).
[3] C. B. Scruby, P. M. Williams, and G. S. Parry, Phil. Mag. **31**, 255 (1975).
[4] B. Sipos, A. F. Kusmartseva, A. Akrap, H. Berger, L. Forró, and E. Tutiš, Nat. Mater. **7**, 960 (2008).
[5] N. Suzuki, A. Yamamoto, and K. Motizuki, J. Phys. Soc. Jpn. **54**, 4668 (1980).
[6] R. Bianco, M. Calandra, and F. Mauri, Phys. Rev. B **92**, 094107 (2015).
[7] T. Kaneko, Y. Ohta, and S. Yunoki, Phys. Rev. B **97**, 155131 (2018).
[8] F. J. Di Salvo, D. E. Moncton, and J. V. Waszczak, Phys. Rev. B **14**, 4321 (1976).
[9] A. Zunger, and A. J. Freeman, Phys. Rev. B **17**, 1839 (1978).
[10] F. Weber, S. Rosenkranz, J.-P. Castellan, R. Osborn, G. Karapetrov, R. Hott, R. Heid, K.-P. Bohnen, and A. Alatas, Phys. Rev. Lett. **107**, 266401 (2011).
[11] D. Jérome, T. M. Rice, and W. Khon, Phys. Rev. **158**, 462 (1967).
[12] Th. Pillo, J. Hayoz, H. Berger, F. Lévy, L. Schlapbach, and P. Aebi, Phys. Rev. B **61**, 16213 (2000).
[13] T. E. Kidd, T. Miller, M.Y. Chou, and T.-C. Chiang, Phys. Rev. Lett. **88**, 226402 (2002).
[14] H. Cercellier, C. Monney, F. Clerc, C. Battaglia, L. Despont, M. G. Garnier, H. Beck, P. Aebi, L. Patthey, H. Berger and L. Forró, Phys. Rev. Lett. **99**, 146403 (2007).
[15] A. Kogar, M. S. Rak, S. Vig, A. A. Husain, F. Flicker, Y. I. Joe, L. Venema, G. J. MacDougall, T. C. Chiang, E. Fradkin, J. van Wezel, P. Abbamonte, Science **358**, 1314 (2017).
[16] M. Holt, P. Zschack, H. Hong, M.Y. Chou, and T.-C. Chiang, Phys. Rev. Lett. **86**, 3799 (2001).
[17] M. Hellgren, J. Baima, R. Bianco, M. Calandra, F. Mauri, and L. Wirtz, Phys. Rev. Lett. **119**, 176401 (2017).
[18] E. Morosan, H. W. Zandbergen, B. S. Dennis, J. W. G. Bos, Y. Onose, T. Klimczuk, A. P. Ramirez, N. P. Ong, and R. J. Cava, Nat. Phys. **2**, 544 (2006).
[19] D. Qian, D. Hsieh, L. Wray, E. Morosan, N. L. Wang, Y. Xia, R. J. Cava, and M. Z. Hasan, Phys. Rev. Lett. **98**, 117007 (2007).
[20] J. F. Zhao, H.W. Ou, G. Wu, B. P. Xie, Y. Zhang, D.W. Shen, J. Wei, L. X. Yang, J. K. Dong, M. Arita, H. Namatame, M. Taniguchi, X. H. Chen, and D. L. Feng, Phys. Rev. Lett. **99**, 146401 (2007).
[21] G. Li, W. Z. Hu, J. Dong, D. Qian, D. Hsieh, M. Z. Hasan, E. Morosan, R. J. Cava, and N. L. Wang, Phys. Rev. Lett. **99**, 167002 (2007).
[22] G. Wu, H. X. Yang, L. Zhao, X. G. Luo, T. Wu, G. Y. Wang, and X. H. Chen, Phys. Rev. B **76**, 024513 (2007).
[23] H. Barath, M. Kim, J. F. Karpus, S. L. Cooper, P. Abbamonte, E. Fradkin, E. Morosan, and R. J. Cava, Phys. Rev. Lett. **100**, 106402 (2008).
[24] Y. I. Joe, X. M. Chen, P. Ghaemi, K. D. Finkelstein, G. A. de la Peña, Y. Gan, J. C. T. Lee, S. Yuan, J. Geck, G. J. MacDougall, T. C. Chiang, S. L. Cooper, E. Fradkin, and P. Abbamonte, Nat. Phys. **10**, 421 (2014).
[25] M. Maschek, S. Rosenkranz, R. Hott, R. Heid, M. Merz, D. A. Zocco, A. H. Said, A. Alatas, G. Karapetrov, S. Zhu, J. van Wezel, and F. Weber, Phys. Rev. B **94**, 214507 (2016).
[26] A. M. Novello, M. Spera, A. Scarfato, A. Ubaldini, E. Giannini, D. R. Bowler, and Ch. Renner, Phys. Rev. Lett. **118**, 017002 (2017).
[27] A. Kogar, G. A. de la Pena, S. Lee, Y. Fang, S. X.-L. Sun, D. B. Lioi, G. Karapetrov, K. D. Finkelstein, J. P. C. Ruff, P. Abbamonte, and S. Rosenkranz, Phys. Rev. Lett. **118**, 027002 (2017).
[28] S. Yan, D. Iaia, E. Morosan, E. Fradkin, P. Abbamonte, and V. Madhavan, Phys. Rev. Lett. **118**, 106405 (2017).
[29] A. F. Kusmartseva, B. Sipos, H. Berger, L. Forró, and E. Tutiš, Phys. Rev. Lett. **103**, 236401 (2009).
[30] L. J. Li1, E. C. T. O'Farrell, K. P. Loh, G. Eda, B. Özyilmaz, and A. H. Castro Neto, Nature (London) **529**, 185 (2016).
[31] A. A. Titov, A. I. Merentsov, A. E. Kar'kin, A. N. Tiov, and V. V. Fedorenko, Phys. Solid State **51**, 230 (2009).
[32] A. S. Shkvarin, Yu. M. Yarmoshenko, N. A. Skorikov, A. A. Tiov, and A. N. Tiov, J. Exp. Theor. Phys. **114**, 324 (2012).
[33] A. S. Shkvarin, Yu. M. Yarmoshenko, M. V. Yablonskikh, A. I. Merentsov, E. G. Shkvarina, A. A. Tiov, Yu. M. Zhukov, and A. N. Tiov, J. Chem. Phys. **144**, 074702 (2016).
[34] K. Sugimoto, H. Ohsumi, S. Aoyagi, E. Nishibori, C. Moriyoshi, Y. Kuroiwa, H. Sawa, and M. Takata, AIP Conf. Proc. **1234**, 887 (2010).
[35] J. P. Perdew, K. Burke, and M. Ernzerhof, Phys. Rev. Lett. **77**, 3865 (1996).
[36] P. Blaha, K. Schwarz, G. K. H. Madsen, D. Kvasnicka, and J. Luitz, *WIEN2K, An Augmented Plane Wave + Local Orbitals Program for Calculating Crystal Properties* (Technical Universität Wien, Austria, 2001).
[37] See Supplemental Material at http://link.aps.org/supplemental/10.1103/PhysRevB.99.081111 for the peak profiles, the raw XRD data, the ordering patterns of Cu atoms, the structural parameters, and the result of the DFT calculation.
[38] R. A. Jishi and H. M. Alyahyaei, Phys. Rev. B **78**, 144516 (2008).
[39] L. Nørdheim, Ann. Phys. (Leipzig) **401**, 607 (1931).

[40] D. A. Papaconstantopoulos and W. E. Pickett, Phys. Rev. B **57**, 12751 (1998).
[41] N. Katayama, S. Tamura, T. Yamaguchi, K. Sugimoto, K. Iida, T. Matsukawa, A. Hoshikawa, T. Ishigaki, S. Kobayashi, Y. Ohta, and H. Sawa, Phys. Rev. B **98**, 081104 (2018).
[42] R.D. Shannon, Acta Crystallogr. **32**, 751 (1976).
[43] Fermi surfaces are visualized using XCRYSDEN, A. Kokalj, Comput. Mater. Sci. **28**, 155 (2003).
[44] The crystal structure is visualized using VESTA, K. Momma, and F. Izumi, J. Appl. Cryst. **44**, 1272 (2011).
[45] T. Takahashi, O. Yamamoto, F. Matsuyama, and Y. Noda, J. Solid State Chem. **16**, 35 (1976).
[46] H. Liu, X. Shi, F. Xu, L. Zhang, W. Zhang, L. Chen, Q. Li, C. Uher, T. Day, and G. J. Snyder, Nat. Mater. **11**, 422 (2012).
[47] J. L. Niedziela, D. Bansal, A. F. May, J. Ding, T. Lanigan-Atkins, G. Ehlers, D. L. Abernathy, A. Said, and O. Delaire, Nat. Phys. **15**, 73 (2019).
[48] K. Takada, H. Sakurai, E. Takayama-Muromachi, F. Izumi, R. A. Dilanian, and T. Sasaki, Nature (London) **422**, 53 (2003).
[49] M. L. Foo, Y. Wang, S. Watauchi, H. W. Zandbergen, T. He, R. J. Cava, and N. P. Ong, Phys. Rev. Lett. **92**, 247001 (2004).
[50] A. Bhide and K. Hariharan, Solid State Ion. **192**, 360 (2011).
[51] I. Terasaki, Y. Sasago, and K. Uchinokura, Phys. Rev. B **56**, 12685(R) (1997).